NRF2 transcriptionally activates the *heat shock factor 1* promoter under oxidative stress and affects survival and migration potential of MCF7 cells

Received for publication, April 9, 2018, and in revised form, October 2, 2018 Published, Papers in Press, October 11, 2018, DOI 10.1074/jbc.RA118.003376

Soumyadip Paul[‡1], **Suvranil Ghosh**[‡1], **Sukhendu Mandal**[§], **Subrata Sau**[§], **and Mahadeb Pal**[‡2]

From the [‡]*Division of Molecular Medicine and* [§]*Department of Biochemistry, Bose Institute, P1/12 CIT Scheme VIIM, Kolkata, India 700054*

Edited by Ursula Jakob

Functional up-regulation of heat shock factor 1 (HSF1) activity through different posttranslational modifications has been implicated in the survival and proliferation of various cancers. It is increasingly recognized that the *HSF1* gene is also up-regulated at the transcriptional level, a phenomenon correlated with poor prognosis for patients with different cancers, including breast cancer. Here, we analyzed the transcriptional up-regulation of *HSF1* in human cells upon arsenite- or peroxide-induced oxidative stress. Sequential promoter truncation coupled with bioinformatics analysis revealed that this activation is mediated by two antioxidant response elements (AREs) located between 1707 and 1530 bp upstream of the transcription start site of the *HSF1* gene. Using shRNA-mediated down-regulation, ChIP of NRF2, site-directed mutagenesis of the AREs, and DNase I footprinting of the *HSF1* promoter, we confirmed that nuclear factor erythroid-derived 2-like 2 (NRF2, also known as NFE2L2) interacts with these AREs and up-regulates *HSF1* expression. We also found that BRM/SWI2-related gene 1 (BRG1), a catalytic subunit of SWI2/SNF2-like chromatin remodeler, is involved in this process. We further show that NRF2-dependent *HSF1* gene regulation plays a crucial role in cancer cell biology, as interference with NRF2-mediated *HSF1* activation compromised survival, migration potential, and the epithelial-to-mesenchymal transition and autophagy in MCF7 breast cancer cells exposed to oxidative stress. Taken together, our findings unravel the mechanistic basis of *HSF1* gene regulation in cancer cells and provide molecular evidence supporting a direct interaction between HSF1 and NRF2, critical regulators of two cytoprotective mechanisms exploited by cancer cells.

Healthy cells up-regulate heat shock factor 1 (HSF1) activity when challenged with a stress such as oxidative stress to protect its normal protein structure and function (1). HSF1 drives expression of a group of inducible heat shock protein chaperones (HSPs) such as HSP70 and HSP90 to refold the affected proteins to their native conformation or drive the removal of aggregates (1–3). HSF1 also controls the up-regulation of many genes associated with different cellular processes other than the HSPs (4–6).

HSF1 exists in unstressed cells in an inactive state within an HSP90-immunophilin-p23 complex (7, 8). Per a current model, a misfolded protein generated under stress titrates away the chaperones from the inactive complex, thereby freeing HSF1 to form a homotrimer. The trimeric complex binds to its recognition sequence, heat shock elements consisting of inverted 5′-nGAAn-3′ motifs on the promoters of its target genes (9). Furthermore, various posttranslational modifications, such as phosphorylation, acetylation, and sumoylation, regulate the activity of HSF1. A noncoding RNA was shown to play an important role in regulating HSF1 function (10, 11). Studies also suggested that HSF1 engages a distinct set of coactivators or corepressors to regulate genes in a stress-specific manner (12).

Normally, cellular HSF1 is inactivated as the stress is ameliorated. In contrast, cancer cells maintain HSF1 in a constitutively activated state to sustain their proliferative potential (13). This event is driven by the relatively higher level of oxidative stress in cancer cells caused by higher NADPH oxidase activity and higher mitochondrial rate of respiration associated with enhanced aerobic glycolysis and a defective antioxidant response (14). Many cancer cells, in particular, maintain an elevated level of the HSPs such as HSP90, HSP70, HSP40, and HSP27 because of overexpression of various oncoproteins. In fact, mice devoid of the *HSF1* gene (*hsf1*−/−) are much less susceptible to chemical-induced transformation (15).

An up-regulated state of the *HSF1* gene in different types of human cancers has been reported (16). *HSF1* mRNA level was significantly up-regulated in oral squamous cell carcinoma, correlating the tumor size with a relatively higher level of HSF1 in the nuclear compartment (17). *HSF1* was found to be overexpressed in the malignant prostate and in pancreatic cancer cells as well (13). Furthermore, *HSF1* gene amplification and higher HSF1 levels were reported in hepatocellular carcinoma (18). Elevated *HSF1* mRNA levels were correlated with higher grades of breast tumors (19). Although all these studies supported transcriptional up-regulation of *HSF1* with cancer growth and proliferation, little is known about the underlying mechanism of this cancer cell–specific *HSF1* regulatory mechanism.

Nuclear factor erythroid-derived 2-like 2 (also named NRF2) controls cellular redox potential in response to oxidative stress

This work was supported by the Science and Engineering Research Board (SERB) and the Department of Biotechnology (DBT), Ministry of Science and Technology and Bose Institute plan program IV. The authors declare that they have no conflicts of interest with the contents of this article.
This article contains Figs. S1–S3 and Tables S1–S3.
[1] Council of Scientific & Industrial Research (CSIR) ad hoc fellows.
[2] To whom correspondence should be addressed. Tel.: 91-33-2569-3256; E-mail: palmahadeb@gmail.com.

(20–22). NRF2 in a healthy cell is constantly degraded through ubiquitination and proteasomal degradation by its association with KEAP1, a substrate adapter protein for the E3 ubiquitin ligase complex. Disruption of its binding with KEAP1 leads to stabilization and nuclear translocation of NRF2. NRF2 binds to the antioxidant response element (ARE)[3] on the promoter of its target antioxidant responsive genes as a heterodimer with a small Maf protein (20, 23–25).

Both NRF2 and HSF1 were reported to control certain genes such as heme oxygenase (26, 27) and *HSP70* (28) associated with cytoprotection. Increasing body of evidence suggested that these two factors also engage in mutual compensatory activities (20). However, it remains to be understood how these activities are precisely regulated.

We investigated *HSF1* promoter regulation under oxidative stress in human cells induced by arsenite treatment as a model (condition) to obtain insight into the phenomenon observed in cancer cells. We identified two AREs in the promoter of the *HSF1* gene responsible for its sensitivity to oxidative stress. We have further shown that the AREs engage in a multiprotein activation complex with NRF2 and the chromatin modifier BRG1 to mediate *HSF1* transcription under arsenic stress. Furthermore, MCF7 cells appear to depend on this NRF2-dependent *HSF1* transcription for their growth and proliferation.

Results

Transcription of the HSF1 gene is up-regulated by a proteotoxic stressor

Up-regulation of the *HSF1* gene was tested in cells in response to two forms of a proteotoxic stressor, heat shock or arsenite treatment. HT1080 cells were either grown at 37 °C (control) or subjected to heat shock (HS) at 42 °C for 1 h or treated with 20 μM sodium arsenite for 2 h. The treated samples were then analyzed for HSP70, HSF1, and GAPDH levels by real-time PCR (qRT-PCR). These two treatment conditions led to a significant induction of HSP70 both at mRNA and protein levels (Fig. 1*A*, *right panel*). An increase in *HSF1* expression notably occurred in arsenite-treated samples only (Fig. 1*A*). Further experimentation will be required to better understand this *HSP70* up-regulation but activation of HSF1 function by differential signaling pathways under these stressors has been reported (12). Notably, *HSP70* was shown to be regulated by a few factors other than HSF1 under HS such as NF-Y, CREB, and NF-κB (29, 30). Up-regulation of *HSF1* (and also its target *HSP70* gene) both at mRNA and protein levels in different cancer cell lines, HeLa, MCF7, and PC3 but not in immortalized cell lines HEK293 and NKE under those treatment conditions measured by qRT-PCR (Fig. 1*B*) and immunoblotting (Fig. 1*C*), respectively, suggested that this is not specific to a particular cancer cell type. ROS, estimated by DCFDA fluorescence (Fig. 1*B*, *right panel*) in response to arsenite treatment, is also higher in MCF7 and HT1080 as compared with HEK293 and NKE cells.

To test whether the increase in *HSF1* mRNA is because of its *de novo* RNA synthesis, and not because of an increased stability, we blocked transcription by treating cells with actinomycin D (ACTD), followed by HS or arsenite treatment as described above. Abrogation of arsenite-induced up-regulation of HSF1 and *HSP70* mRNA and protein levels upon ACTD treatment suggested that *HSF1* was indeed up-regulated at the transcriptional level by arsenite (Fig. 1*D*).

Identification of sequence elements present in the HSF1 gene promoter responsible for its up-regulation by arsenite treatment

To locate the enhancer element, several truncated versions of *HSF1* gene promoter DNA, along with the full-length version, were cloned upstream of the Renilla luciferase reporter in a promoterless pGL4.79 vector (Fig. 2*A*, *left panel*). The full-length promoter construct carries the *HSF1* promoter sequence from −1931 to +78 (+1, transcriptional start site) (pHSF1-FL (−1931/+78)). A reporter construct pHSP70 (−450/+91) carrying from −450 to +91 bp of the *HSP70A1A* promoter in the same vector was used as a positive control. The empty vector was used as a negative control. As revealed by luciferase mRNA level measured by qRT-PCR, cells transfected with pHSF1-FL (−1931/+78) construct showed >7-fold induction with arsenite treatment (Fig. 2*A*, *right panel*). HT1080 cells were chosen for this study because of a relatively low basal level of *HSF1* mRNA in them. Assay of other constructs upon an identical treatment condition revealed that the region between −1720 and −1360 is responsible for the observed effect (Fig. 2*A*, *right panel*). To identify transcription factors that can bind this region, the nucleotide sequence of *HSF1* promoter spanning from −1931 to −1360 nucleotides was subjected to transcription factor–binding site analysis by rVista (rVista 2.0, https://rvista.dcode.org)[4] (71). This analysis predicted binding sites for hundreds of transcription factors including three putative binding sites of NRF2, a transcription factor reported to be up-regulated with oxidative stress (22, 31–33). However, there was no prediction for the presence of any heat shock element motif with confidence (data not shown). NRF2, a basic leucine zipper (bZIP) protein binds to AREs upon oxidative stress in the upstream promoter region of many antioxidative phase II genes like *NQO1*, *HO-1*, and *TRX* (34). The putative NRF2-binding sites ARE-A, ARE-B, and ARE-C on the *HSF1* promoter including their predicted scores are shown (Fig. 2*B*). The nucleotide sequence in capital letters highlights the core-binding regions. Comparison of the consensus ARE sequence with those of *HSF1*, *NQO1*, and *HO-1* gene promoters using Clustal Omega multiple sequence alignment tool identified distinct types of *HSF1* AREs (Fig. 2*C*) (35–39).

Effect of NRF2 knockdown on HSF1 expression

To check the dependence of NRF2 for *HSF1* induction by arsenite, HT1080 cells were transiently transfected with shRNA

[3] The abbreviations used are: ARE, antioxidant response element; HS, heat shock; RA, retinoic acid; qRT, quantitative/real-time; ROS, reactive oxygen species; DCFDA, 2′,7′-dichlorodihydrofluorescein diacetate; ACTD, actinomycin D; NAC, *N*-acetyl cysteine; EMT, epithelial-mesenchymal transition; PBST, 137 mM NaCl, 2.7 mM KCl, 10 mM Na_2HPO4, 1.8 mM KH_2PO4, pH 7.4, supplemented with 0.1% Tween 20; mCMV, minimal cytomegalovirus; NE, nuclear extracts; Rluc, Renilla-luciferase; MTT, 3-(4,5-dimethylthiazol-2-yl)-2,5-diphenyltetrazolium bromide.

[4] Please note that the JBC is not responsible for the long-term archiving and maintenance of this site or any other third party hosted site.

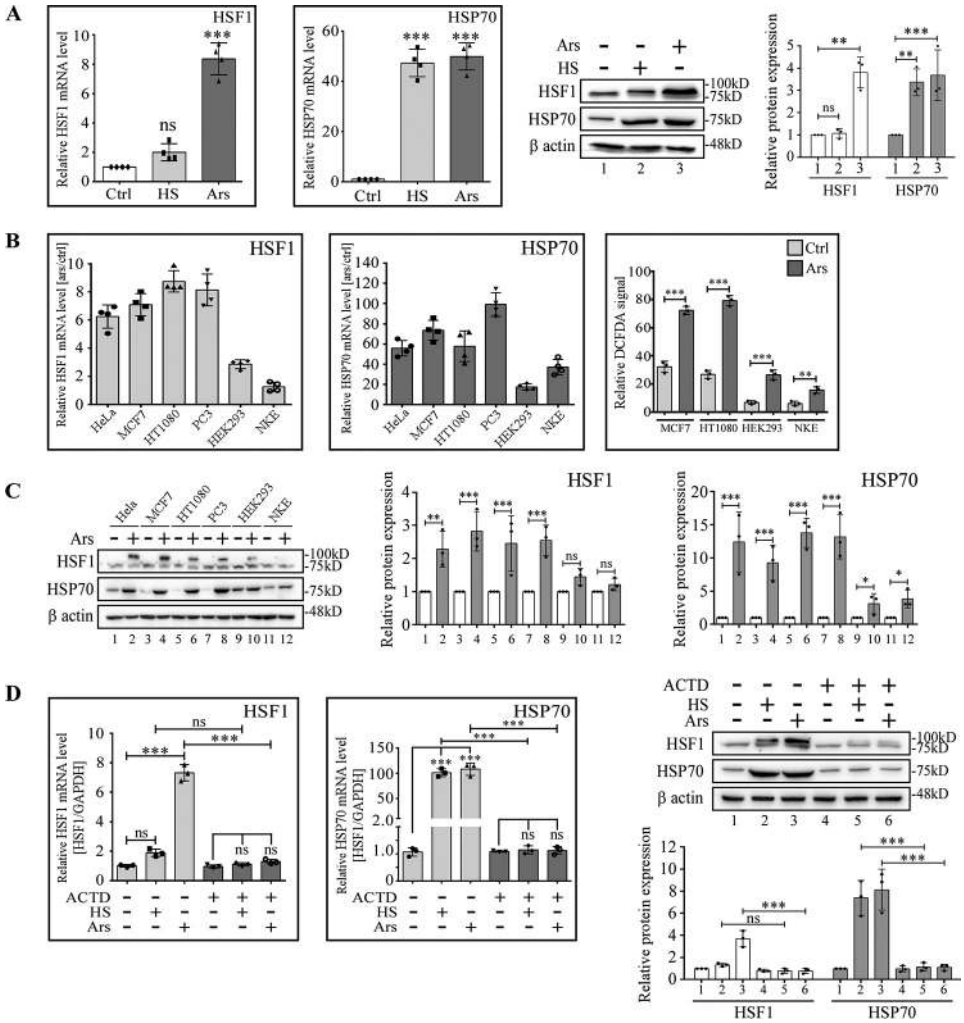

Figure 1. Transcriptional up-regulation of *HSF1* and *HSP70* genes in cells of different organ origin upon arsenite treatment. *A*, qRT-PCR analysis of HSF1 and *HSP70* mRNA levels in HT1080 cells upon heat shock at 42 °C for 1 h (*HS*) or exposure to 20 μM arsenite for 2 h (*Ars*) represented by scatter plots. *Error bar*, mean ± S.D. ($n = 4$); *ns*, not significant; ***, $p < 0.001$ compared with control (*Ctrl*). Representative immunoblots showing the up-regulation HSF1 and HSP70 in HT1080 cells as indicated with estimation of their levels shown on the *right*. *Error bar*, mean ± S.D. ($n = 3$); *ns*, not significant; **, $p < 0.01$; ***, $p < 0.001$. *B*, qRT-PCR analysis of *HSF1* and *HSP70* mRNA levels upon arsenite treatment in different cell lines as indicated (*left* and *middle panels*). Estimation of relative ROS levels induced in different cell lines under conditions indicated as determined by DCFDA assay, performed after 2 h of arsenite treatment (*right panel*). *Error bar*, mean ± S.D. ($n = 3$); **, $p < 0.01$; ***, $p < 0.001$, compared with Ctrl. *C*, representative immunoblots showing the up-regulation of HSF1 and HSP70 in different cell lines as indicated with estimations of their levels as shown on the *right*. *Error bar*, mean ± S.D. ($n = 3$); *ns*, not significant; *, $p < 0.05$; ***, $p < 0.001$. *D*, qRT-PCR analysis of *HSF1* and *HSP70* mRNA in HT1080 cells pre-treated with or without 1 μg/ml ACTD for 2 h followed by treatment with HS or arsenite. In all assays, GAPDH mRNA level was used as normalization control. Representative immunoblots show the up-regulation *HSF1* and *HSP70* as indicated with estimation of their levels shown on the *right*. In all immunoblot experiments β-actin was used as internal reference. *Error bar*, mean ± S.D. ($n = 3$); ***, $p < 0.001$; *ns*, not significant.

against *NRF2* or a scramble (pLKO.1-shNRF2 *versus* pLKO.1-scr) to knock down endogenous *NRF2*. qRT-PCR analysis suggested that down-regulation of NRF2 prevented induction of *HSF1* expression by arsenite (Fig. 3*A*). Efficient knockdown of NRF2 as determined by immunoblot (Fig. 3*B*) was reflected in inhibition of *HO-1* gene expression (Fig. 3*A*, *lower panel*). Inhibition of arsenite-induced *HSF1* expression under this condition was also shown by immunoblotting (Fig. 3*C*). Interestingly, the *HSP70* transcript level under the same treatment condition was decreased to a lesser extent, which may reflect compensatory role of HSF1 for NRF2 (see "Discussion").

Functional validation of putative NRF2-binding sites in the HSF1 promoter

To functionally validate the importance of three putative ARE motifs on *HSF1* promoter activity, reporter constructs were made in pGL4.79-mCMV vector, where one of these motifs (ARE-A, -B, or -C) was deleted one at a time (Fig. 3*D*). The NQO1-ARE was cloned in the same vector and used as an NRF2-sensitive positive control. *HSP70* promoter cloned in the same vector was also used in the assay. Luciferase expression obtained (by assaying the luciferase mRNA levels) from these ARE-carrying constructs were then compared with a pHSF1-FL construct (Fig. 3*D*, *left panel*). As shown (Fig. 3*D*, *middle panel*), ARE-B and ARE-C are important for NRF2-dependent *HSF1* up-regulation. When compared with the full-length reporter expression, deletion of ARE-B (compare pHSF1–ARE-C with pHSF1-FL; also compare pHSF1–ARE-C with pHSF1–ARE-BC) or ARE-C (compare pHSF1–ARE-AB with pHSF1-FL) reduced luciferase expression most, whereas deletion of ARE-A (compare pHSF1–ARE-BC with pHSF1-FL) did not significantly affect reporter induction by arsenite. Deletion of

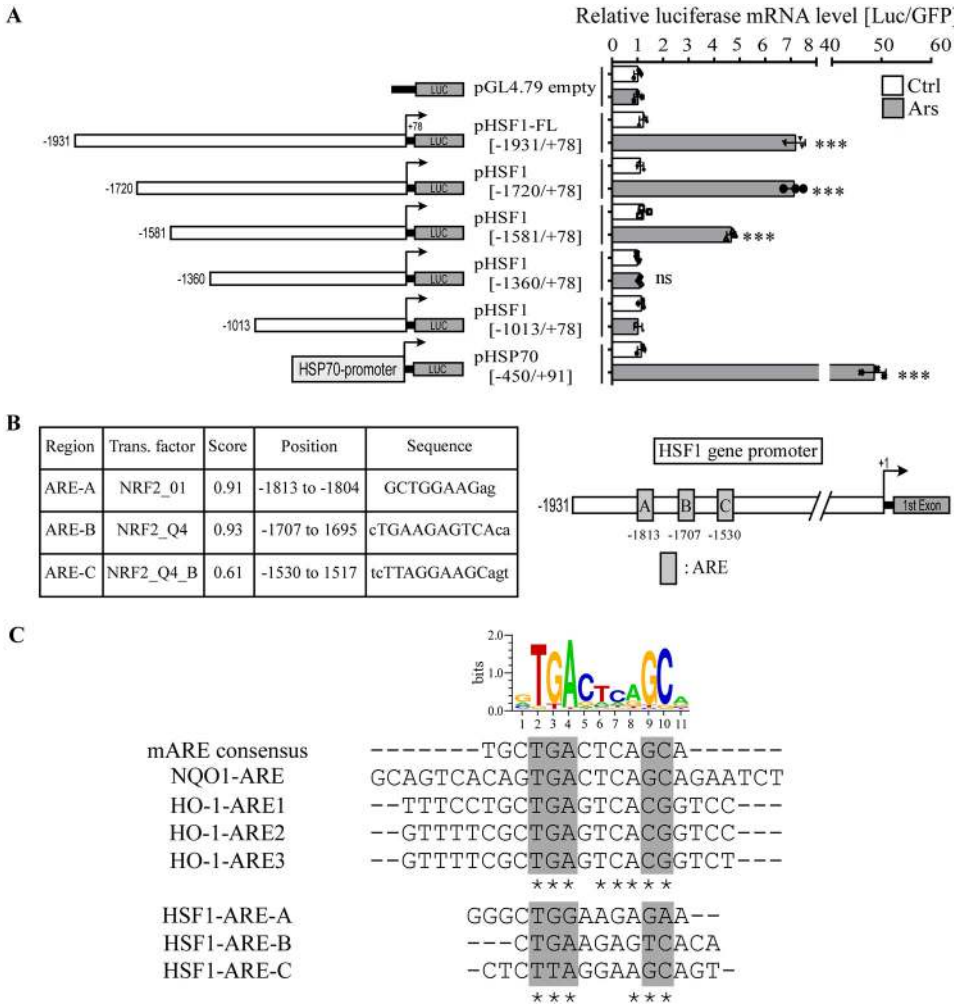

Region	Trans. factor	Score	Position	Sequence
ARE-A	NRF2_01	0.91	-1813 to -1804	GCTGGAAGag
ARE-B	NRF2_Q4	0.93	-1707 to 1695	cTGAAGAGTCAca
ARE-C	NRF2_Q4_B	0.61	-1530 to 1517	tcTTAGGAAGCagt

Figure 2. Analysis of *HSF1* gene promoter elements responsible for its sensitivity to arsenite treatment. *A*, luciferase reporter assay was performed in HT1080 cells using full-length and different truncated versions of the *HSF1* promoter as indicated by schematic drawing. Numbers indicate nucleotide positions with respect to +1 as the transcriptional start site. qRT-PCR analysis of promoter activity (-fold increase in luciferase mRNA level) in arsenite-treated *versus* untreated samples expressed as relative luciferase mRNA levels represented by scatter plots. *Error bar*, mean ± S.D. ($n = 3$); ***, $p < 0.001$; *ns*, not significant. Relative luciferase mRNA level was normalized by measuring GFP mRNA level from a vector cotransfected with the reporter vector as a transfection control. *B*, putative AREs with corresponding scores, locations, and core sequences on the *HSF1* promoter as revealed by rVISTA analysis (*left panel*). Schematic shows putative AREs with their relative positions on the *HSF1* promoter (*right panel*). *C*, Clustal Omega alignment of nucleotide sequences of *HSF1* promoter AREs with those of *NQO1* and *HO-1* promoters. The nucleotides matching the logo generated by the WebLogo program are marked by *asterisks*.

either ARE-B or ARE-C reduced the reporter expression level by ~49 and ~46%, respectively (Fig. 3*D*, *middle panel*). Notably, cells with down-regulated NRF2 showed a significant loss of reporter expression in all of the *HSF1*-promoter constructs (Fig. 3*D*, *middle* and *right panels, open arrow*) like NQO1-ARE-Luc construct (Fig. 3*D*, *middle* and *right panels, solid arrow*). These results suggest that NRF2 is involved in the induction of *HSF1* gene expression by arsenite which acts through the ARE-B and ARE-C motifs.

NRF2 binds to predicted AREs of the HSF1 promoter in vitro

Electrophoretic mobility shift assay (EMSA) was carried out to examine the binding of NRF2 to ARE-A, ARE-B, and ARE-C elements of the *HSF1* promoter. These motifs, along with their mutant versions were synthesized individually as 26-bp double-stranded oligonucleotides and labeled at their 5′-ends with [γ-^{32}P]ATP (used as probes). Nuclear extract (Nuc) isolated from HT1080 cells, untreated or pretreated with arsenite, were used as the source of NRF2 protein. Formation of arsenite-induced DNA-protein complex could be detected only with WT ARE-B and ARE-C (compare Fig. 4*A*, *lane 5* with *lane 7*, and *lane 9* with *lane 11*; *arrowhead*). Both ARE-B and ARE-C, like NQO1-ARE (positive control), formed DNA-protein complexes only with arsenite-treated nuclear extract (Fig. 4*B*, *lanes 3*, *7*, and *11*; *arrowhead*). As expected, all three ARE-B, ARE-C, and NQO1-ARE formed similar complexes as suggested by their similar mobility. Addition of a 100-fold molar excess of respective unlabeled probes abolished the formation of complexes (Fig. 4*B*, *lanes 5*, *9*, and *13*). An inclusion of NRF2-specific antibody in the reaction resulted in supershifting of the labeled complexes (Fig. 4*B* *lanes 4*, *8*, and *12*; compare the *filled arrowhead* with an *open one*). Addition of a nonspecific IgG instead of α-NRF2 antibody in the reaction did not produce any effect on the mobility of the complex (Fig. S2).

NRF2 binds an ARE as a heterodimer with a small Maf protein to elicit its transactivation function (31, 33). Binding to an

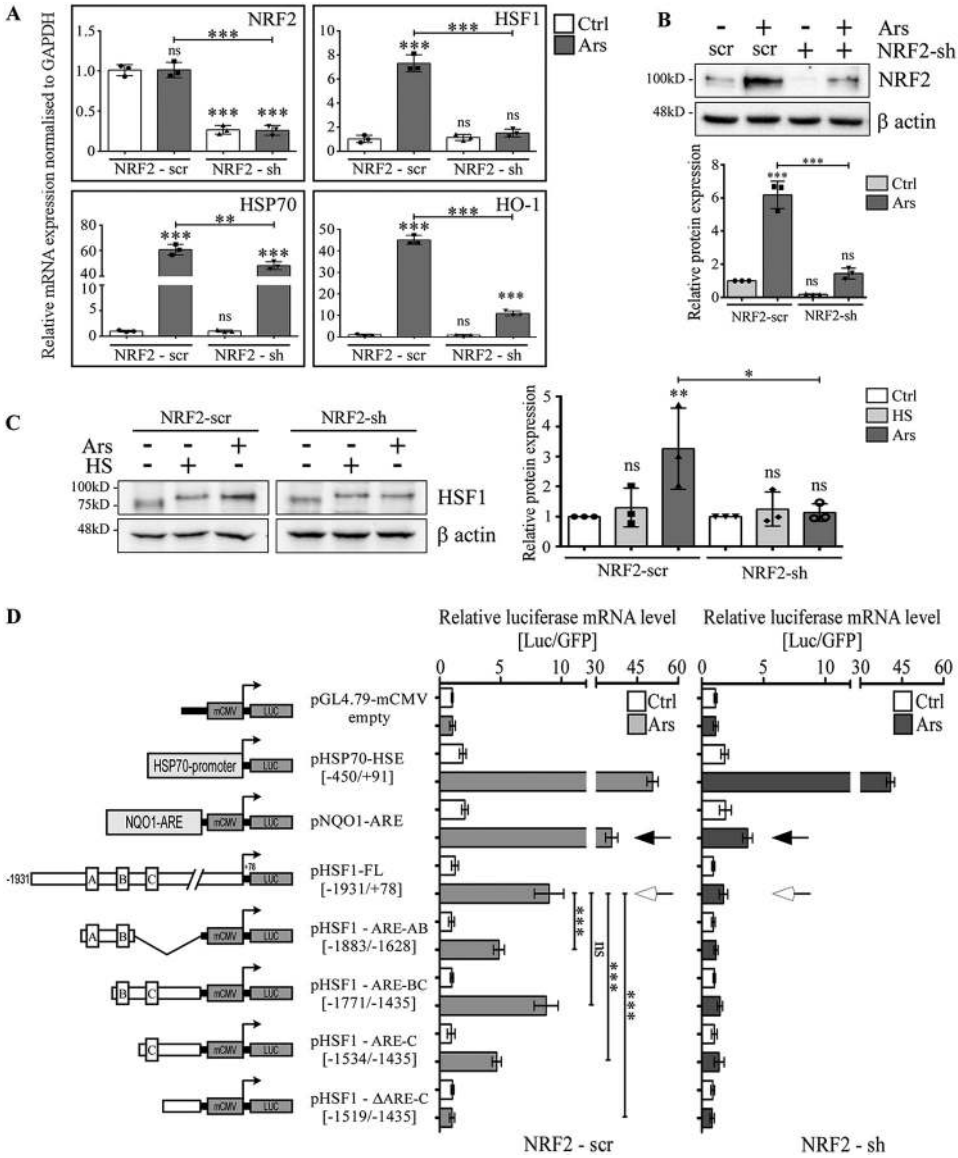

Figure 3. NRF2 regulates *HSF1* transcription by arsenite treatment in HT1080 cells. *A*, qRT-PCR analysis of the effect of shRNA-mediated *NRF2* knockdown on arsenite (*Ars*)-induced *HSF1* expression and other genes as indicated. *Error bar*, mean ± S.D. ($n = 3$); *ns*, not significant; ***, $p < 0.001$ compared with Ctrl-NRF2-scr. *B*, representative immunoblots showing the levels of NRF2 along with estimation of their levels as indicated. *Error bar*, mean ± S.D. ($n = 3$); *ns*, not significant; ***, $p < 0.001$ compared with Ctrl-NRF2-scr. *C*, representative immunoblots showing the levels of HSF1 along with estimation of their levels as indicated. *Error bar*, mean ± S.D. ($n = 3$); df **, $p < 0.01$ compared with Ctrl-NRF2-scr column. *D*, schematic showing *HSF1* promoter-luciferase constructs employed to functionally validate each of the putative AREs located on the *HSF1* promoter (*left panel*), and their dependence on NRF2 by luciferase reporter assay (*right panels*). Relative promoter activity is expressed as the ratio between the mRNA levels of luciferase and GFP mRNAs, with or without *NRF2* knockdown (*NRF2-sh*). *Solid arrow* and *open arrows* point the effect on NQO1-promoter and HSF1-promoter activities, respectively. *Error bar*, mean ± S.D. ($n = 3$); *ns*, not significant; ***$p < 0.001$ compared with pHSF1-FL+ars column.

ARE sequence was tested with a purified His_6-NRF2 and His_6-MafG protein mixed together in varying molar ratios. NRF2 with MafG in the molar ratio of 1:2 resulted in a visible complex with all the AREs (Fig. 4*C*, *lanes 4*, *7*, and *10*, *arrowhead*). The complexes formed on *NQO1*-ARE (using this ratio of NRF2 and MafG) were challenged with increasing concentrations of unlabeled *NQO1*-ARE, ARE-B, and ARE-C. As revealed, complex assembled on the ARE-C was less stable than that on the *NQO1* and ARE-B (Fig. 4*D*). Direct measurement of the equilibrium dissociation constant (K_D) suggested the complex formed on ARE-B is of higher stability compared with that on ARE-C with K_D of 0.983 μM and 1.847 μM, respectively, whereas the K_D of the complex formed on the *NQO1*-ARE was 0.672 μM (Fig. 4*E*).

A direct association of NRF2-MafG with the AREs is also reflected in the DNase I footprinting assay. As revealed, protection by the complex to DNase I digestion extended to nucleotides beyond the core motifs of all three AREs including the *NQO1* (Fig. 4*F*). Interestingly, binding of NRF2-MafG complex induced DNase I hypersensitivity only at the ARE-B (*asterisk*).

NRF2 interacts with HSF1 promoter AREs in cells

Redox imbalance activates NRF2 in a cell which should in principle be neutralized by a ROS quencher, *N*-acetyl cysteine (NAC). This was essentially found when internal ROS levels were measured (Fig. 5*A*).

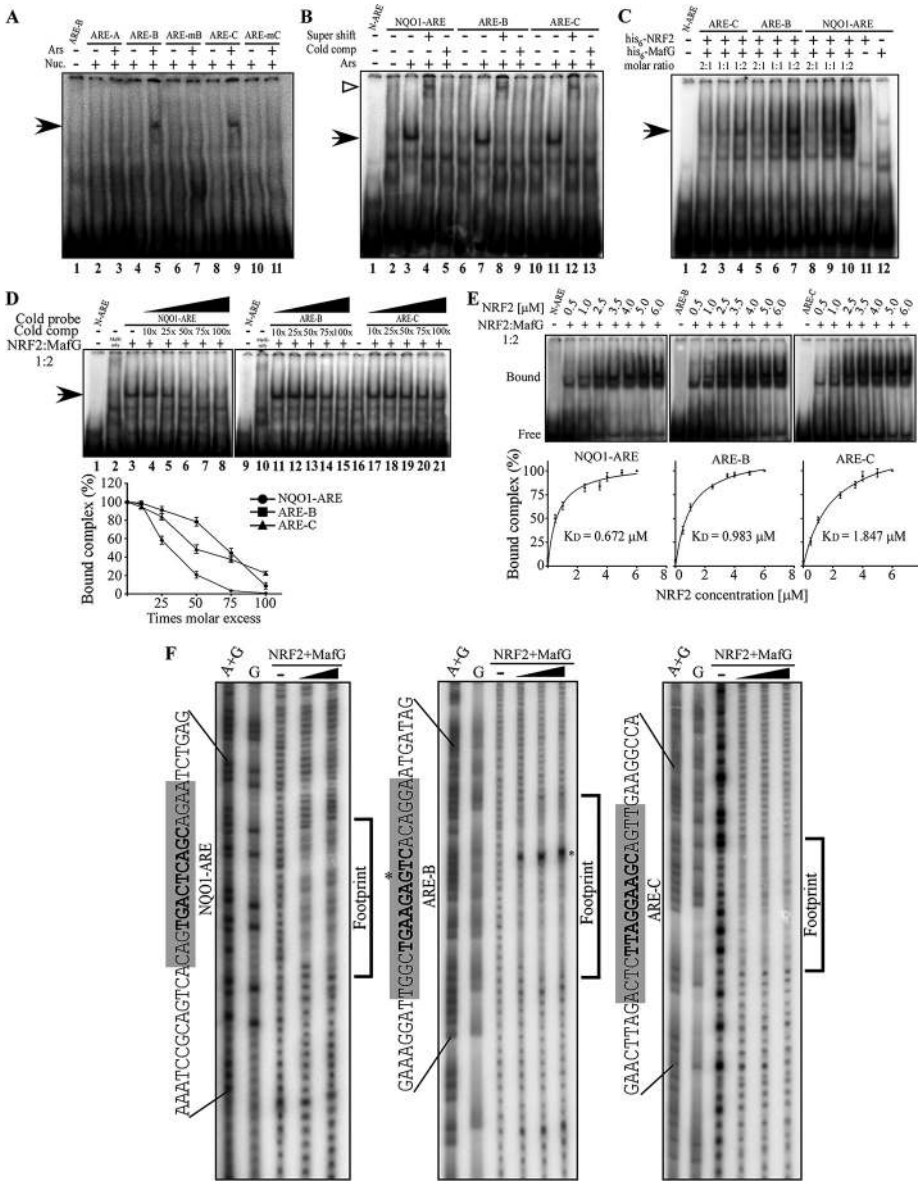

Figure 4. NRF2 binds putative ARE-regions identified in the *HSF1* gene promoter. *A*, EMSA demonstrating the formation of protein-DNA complex (*arrowhead*) only with WT *HSF1* ARE-B and ARE-C oligonucleotides as probes, but not with ARE-A or with mutated AREs (ARE-mB and ARE-mC). Nuclear extract (*Nuc*) isolated from HT1080 cells pretreated with arsenite (*Ars*) was used in the experiment. *B*, EMSA showing complex formation on ARE-B and ARE-C with the same *Nuc* used in *panel A* along with *NQO1*-ARE used as positive control. One hundred–fold excess of unlabeled oligonucleotide over its labeled counterpart was used in the cold competition experiment (*cold comp*). Complexes super-shifted with NRF2 antibody are indicated (*open arrowhead*). *C*, EMSA showing the effect of different molar ratios of purified NRF2 and MafG proteins used in the formation of the complex on the indicated AREs. *D*, EMSA for comparison of the relative affinity of the AREs for complex formation. Complexes were formed on *NQO1*-ARE by purified NRF2:MafG and challenged by different molar excess of the unlabeled corresponding double stranded oligonucleotides (*cold probe*) as indicated. *Lower panel*, plots showing the sensitivity of the complexes (estimated by densitometric scanning of corresponding bands) to increasing doses of unlabeled AREs as indicated. *Error-bar*, mean ± S.D. ($n = 3$). *E*, EMSA and corresponding plots showing measurement of the equilibrium dissociation constant (K_D). The percentage of bound complex formed on each of *NQO1*-ARE, ARE-B, and ARE-C DNA is plotted as a function of the monomeric concentration of purified NRF2. The K_D of each complex is indicated. *Error bar*, mean ± S.D. ($n = 3$). *F*, autoradiogram showing DNase I footprints of NRF2 binding on the top strands of *NQO1*-ARE, ARE-B, and ARE-C motifs. DNase I–protected regions are *shaded*, with the ARE sequence shown in *bold letters*. Lanes *A*+*G* and *G* contain the products of Maxam-Gilbert chemical sequencing reactions for dA and dG residues that served as sequence markers. *Asterisk*, hypersensitive site.

To test if NRF2 is recruited to the AREs on the *HSF1* promoter, chromatin immunoprecipitation (ChIP) analysis was performed in cells pretreated or untreated with arsenite in the presence or absence of NAC. For convenience, cells overexpressing FLAG-NRF2 were used. In the assay, ChIP-enriched DNA carried ARE-B and ARE-C regions only and *NQO1*-ARE (positive control), but not that of ARE-A. This was greatly reduced by NAC pre-treatment. This indicated that NRF2 associates only with ARE-B and ARE-C upon arsenite treatment. Results are summarized by bar graphs where enrichment of the untreated control samples was defined as 1 (Fig. 5*B*).

Increase in arsenite-induced *HSF1* mRNA expression depended on ROS generation. Expression of HO-1, an NRF2 target gene, was monitored as a positive control in the experiment (Fig. 5*C*). Tertiary butylhydroquinone (TBHQ), an inducer of mitochondrial oxidative stress and NRF2 activity (40), effec-

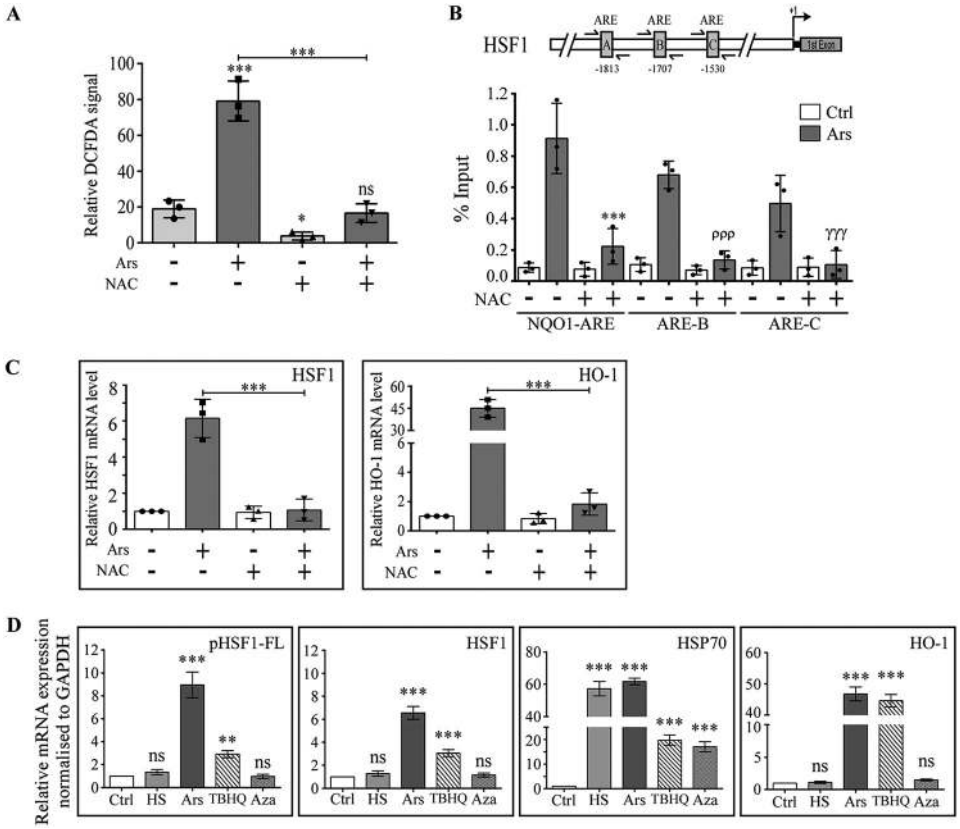

Figure 5. NRF2 binds HSF1 AREs in cells. *A*, analysis of the effect of *N*-acetyl cysteine (NAC) in quenching ROS generated in MCF7 cells. Estimation of relative ROS levels induced under conditions indicated as determined by DCFDA assay, performed after 2 h of arsenite treatment. *Error bar*, mean ± S.D. ($n = 3$); ***, $p < 0.001$; *, $p < 0.05$ compared with Ars-NAC column. *B*, relative enrichment of NRF2 on the indicated AREs in MCF7 cells pre-transfected with pcDNA-based FLAG-NRF2 expression constructs with or without NAC pre-treatment, as estimated by ChIP assay. The schematic on top shows the position of the primers used in the ChIP experiment. *Error bar*, mean ± S.D. ($n = 3$); ***, $p < 0.001$ compared with *NQO1*-ARE −NAC+Ars column; ρρρ, $p < 0.001$ compared with ARE-B −NAC+Ars column; γγγ, $p < 0.001$ compared with ARE-C −NAC+Ars column. *C*, qRT-PCR analysis showing the effect of NAC on arsenite-induced *HSF1* gene transcription in HT1080 cells. *Error bar*, mean ± S.D. ($n = 3$); ***, $p < 0.001$ compared with −Ars-NAC column. *D*, qRT-PCR analysis showing the response of different genes to various stressors as indicated. Tertiary butylhydroquinone (*TBHQ*) and azadiradione (*Aza*) were used at 100 μM and 10 μM for 16 h, respectively. Full-length (*FL*) *HSF1*-promoter-luciferase construct was used in the experiment as an internal reference. *Error bar*, mean ± S.D. ($n = 3$); **$p < 0.01$, ***$p < 0.001$ compared with untreated control; *ns*, not significant.

tively induced *HSF1* promoter activity as tested by assaying the sensitivity of the *HSF1* promoter–directed reporter and endogenous *HSF1* mRNA levels (Fig. 5*D*). Azadiradione, an inducer of HSF1 activity (41), had little effect on *HSF1* mRNA and HO-1 levels, although it significantly induces *HSP70* mRNA (Fig. 5*D*). *HSF1* mRNA induction is, therefore, a direct consequence of NRF2 activity caused by oxidative stress.

Arsenite-induced HSF1 up-regulation requires chromatin remodeler BRG1

NRF2, a member of the cap 'n' collar family of transcription factors, recruits CREB binding protein coactivator to its target gene promoters through cooperative interaction of its two domains Neh4 and Neh5 in a stress-independent manner (42, 43). The Neh3 domain of NRF2 was shown to recruit CHD6 to the *NQO1* gene both under basal and *tert*-butylhydroquinone induction (44). A BRG1-containing coactivator was shown to be required for NRF2-dependent activation of the *HO-1*, but not *NQO1* gene (45). A possible involvement of a chromatin-remodeling complex on the *HSF1* promoter was tested by measuring the effect of down-regulation of subunits of different chromatin-remodeling complexes such as SSRP1 of the FACT complex, BRG1 (SMARCA4) of the SWI2/SNF2 complex, and SMARCA3 of the SWI/SNF complex (HLTF) using corresponding siRNAs or shRNAs (Fig. 6*A*). Among these, only BRG1 down-regulation affected arsenite-mediated *HSF1* expression to a significant level (Fig. 6*B*). Reduced recruitment of RNA-polymerase II specifically to the promoter region of *HSF1* (HSF1-pr) upon BRG1 inhibition, is indicative of NRF2 dependence on BRG1 for its function in response to arsenite stress (Fig. 6*C*).

Effect of NRF2-dependent HSF1 expression on proliferation and epithelial to mesenchymal transition of MCF7 cells induced by oxidative stress

Up-regulation of *HSF1* gene expression at the levels of protein and mRNA was reported in breast cancer patients by a cohort study (19, 46). Therefore, MCF7 cells were selected to validate the importance of NRF2-dependent *HSF1* expression in a cellular function. HSF1 and NRF2 functions were down-regulated by shRNA or all-*trans* retinoic acid (RA), respectively, alone or in combination, to assess their effects on cell morphology, proliferation, viability, as well as epithelial-mesenchymal transition (EMT) of MCF7 cells in response to arsenite treatment. NRF2 in the presence of RA is defective in ARE binding because it preferably forms complex with retinoic acid receptor α when RA is present (47). The optimum concentra-

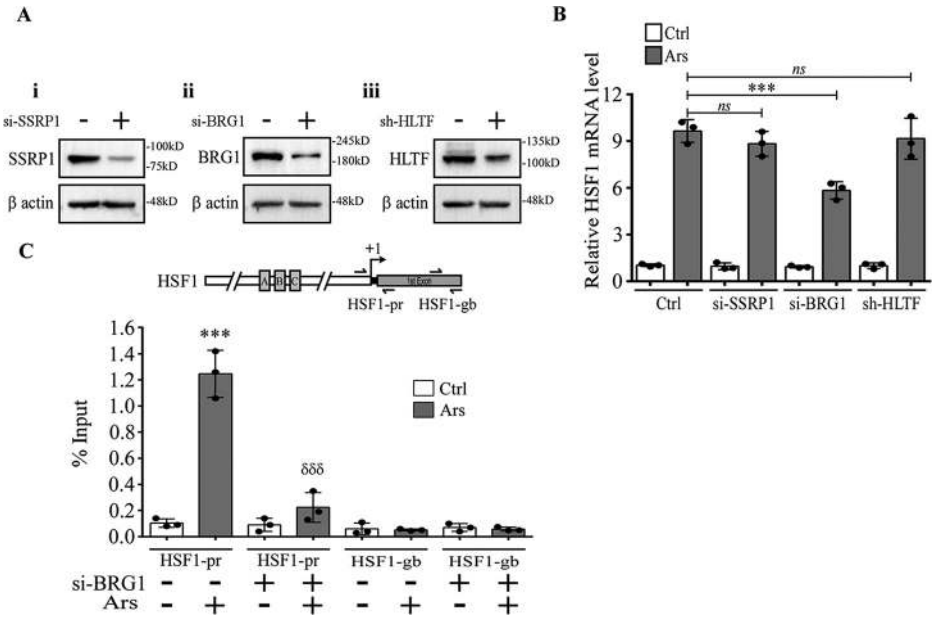

Figure 6. Arsenite-induced *HSF1* transcription requires BRG1, but not HLTF or SSRP1, in MCF7 cells. *A*, representative immunoblots showing knockdown levels of the indicated factors with their corresponding siRNA and shRNA. *B*, qRT-PCR analysis showing the levels of *HSF1* mRNA by arsenite treatment with the indicated factors down-regulated. *Error bar*, mean ± S.D. ($n = 3$); ***, $p < 0.001$. *C*, ChIP qPCR analysis of RNAP II recruitment by arsenite treatment on the *HSF1* promoter (*HSF1-pr*) in cells pretreated with siBRG1. The position of the primers used in the ChIP experiment was shown on the top. *Error bar*, mean ± S.D. ($n = 3$); ***, $p < 0.001$ compared with −siBRG1-Ars; δδδ, $p < 0.001$ compared with −siBRG1+Ars. *Error bar*, mean ± S.D.; *ns*, not significant. HSF1-pr, *HSF1* gene promoter; HSF1-gb, gene body.

tion of RA on NRF2 function inhibition was determined by its dose-dependent activity, *i.e.* inhibition *versus* toxicity study (Fig. S1). Dependence of MCF7 cells to NRF2-dependent *HSF1* transcription demonstrated a drastic change in their morphology; MCF7 developed apoptotic vesicles when exposed to arsenite as well as when treated with *HSF1* shRNA and RA (Fig. S3, *arrows*). Inhibition of the factors NRF2 and HSF1, alone or in combination, also resulted in a marked alteration in the proliferation (Fig. 7*A*) and the viability (Fig. 7*B*) of the cells (Fig. 7*C*, Fig. S3). Similar effect on *HO-1* expression by arsenite treatment in cells pre-treated with RA or NRF2 shRNA suggested that these two treatments are functionally comparable (Fig. 7*C*). EMT, a crucial developmental event in cells, has been shown to correlate with the aggressiveness of cancer (48). To further assess the effect of *HSF1* and *NRF2* inhibition on tumorigenicity, the expression levels of two important EMT markers, E-cadherin and N-cadherin, were determined by immunoblotting (49, 50). After 4 days of arsenite exposure, E-cadherin, an epithelial marker, decreased in the arsenite-treated set, but not so when both HSF1 and NRF2 were inhibited (Fig. 7*D*). The arsenite-induced up-regulation of mesenchymal marker N-cadherin, in contrast, was abrogated following inhibition of HSF1 and NRF2 (Fig. 7*D*).

Autophagy was earlier shown to help cancer cell survival and migration through overcoming intracellular and extracellular stress (51). To examine if autophagy has any role in this case, immunoblotting was carried out to estimate the level of LC3II, a marker of autophagy activation (52). The level of ATG7, a HSF1 target (53) and an E1 ubiquitin ligase involved in the autophagosome formation (54), was also monitored. Inhibition of HSF1 and NRF2 alone or in combination appeared to affect the levels of LC3II (Fig. 7*D*). Next, role of ATG7 and HSF1 alone and in combination was analyzed. The results suggested that down-regulation of these factors which inhibit autophagy also impairs EMT (Fig. 7*E*). Involvement of NRF2 and HSF1 in cell migration in response to arsenite treatment was monitored by wound healing assay. Significant block in migration/wound healing of cells was observed when both the factors were inhibited (Fig. 7*F*). Induction of *HSF1* by peroxide treatment was found to be similarly dependent on NRF2, as RA treatment reduced *HSF1* mRNA transcription similar to that in the *HO-1* gene (Fig. 7*G*, S1*B*). The role of HSF1 and NRF2 on cell viability was also measured in response to hydrogen peroxide treatment yielding results similar to that of arsenite (Fig. 7*H*).

Discussion

Results presented here have unraveled a molecular basis of transcriptional up-regulation of cellular *HSF1* gene by NRF2 upon oxidative stress induced by sodium arsenite or hydrogen peroxide (Figs. 1 and 7, *G* and *H*). Two AREs located between 1707 and 1517 bp upstream of the *HSF1* promoter were identified to be responsible for mediating the NRF2 function (Figs. 2 and 3). We also showed that this event plays an important role in survival, proliferation, and migration of breast cancer cells (Fig. 7). Constitutive activation of NRF2 has been implicated by earlier studies in cancer cell survival and proliferation (32, 55).

An important finding of this study is the identification of two unique AREs by comparison with an up-to-date consensus ARE-sequences. Although the sequence analysis software identified ARE-A, ARE-B, and ARE-C, functional assays validated only ARE-B and ARE-C as the functional AREs. These two AREs differed from that of the *NQO1* or *HO-1* gene (Fig. 2*C*). For example, the ARE-B element matched the upstream TGA present in both *NQO1* and *HO-1* AREs but not downstream.

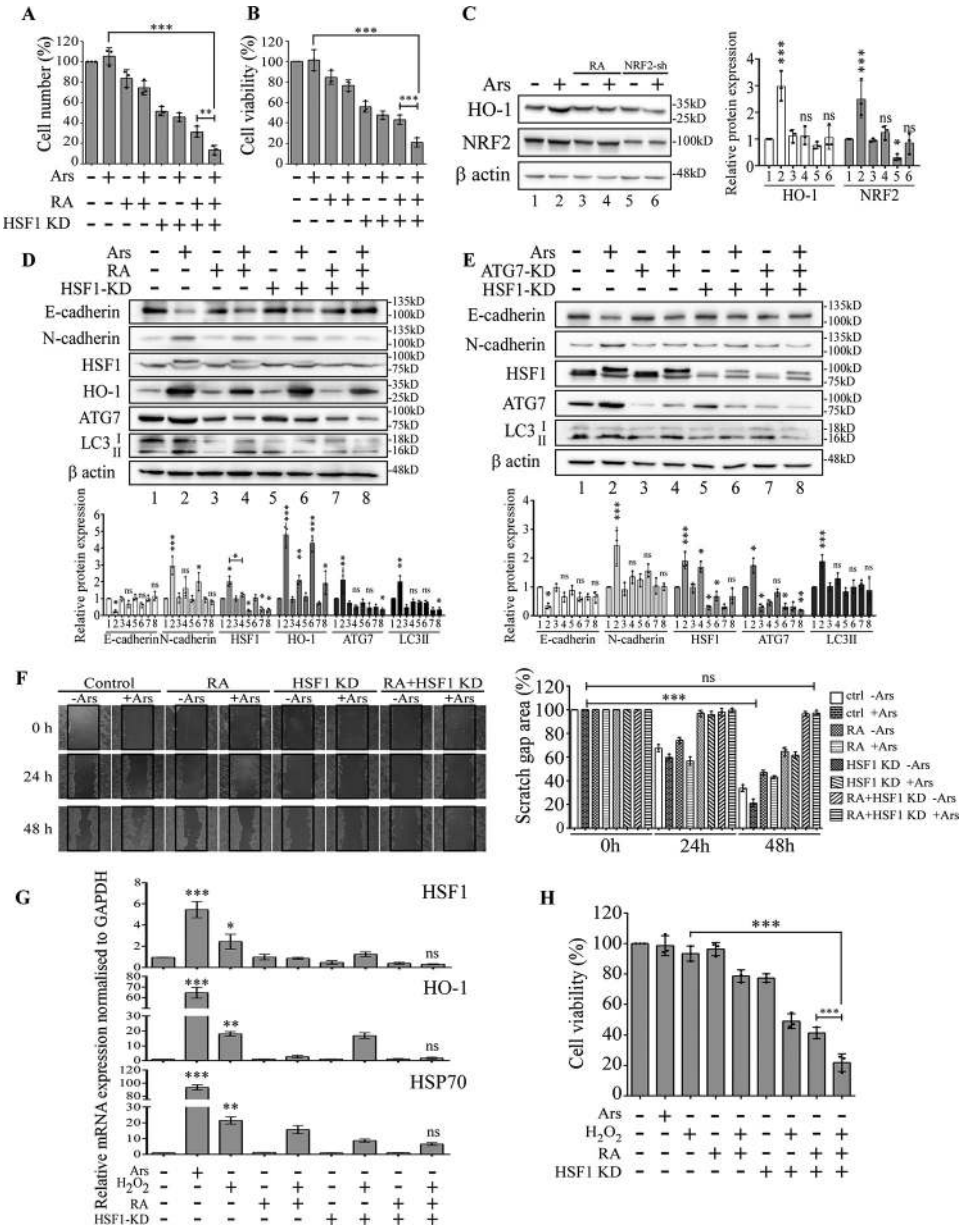

Figure 7. NRF2 regulation of *HSF1* is required for biology in MCF7 cells upon stress induced by arsenite and peroxide treatment. *A* and *B*, levels of growth and viability of MCF7 cells upon *HSF1* inhibition by shRNA (HSF1-KD) and NRF2 inhibition by all-*trans* RA determined by cell counting (*A*) and MTT assay (*B*), respectively. *Error bar*, mean ± S.D. ($n = 3$); ***, $p < 0.001$. *C*, representative immunoblots along with estimation of their levels showing relative efficiency of RA and *NRF2*-shRNA in inhibiting NRF2 function. *D*, representative immunoblots along with estimation of their levels showing the roles of HSF1 and NRF2 in EMT. The EMT markers and efficacy of HSF1-KD are indicated. Cells were pre-treated with 1 μM arsenite for 4 days before EMT markers were checked. *E*, representative immunoblots along with estimation of their levels showing the effect of ATG7 and HSF1 on autophagy and EMT. *F*, effect of ablation of HSF1 and NRF2 functions on cell migration and wound healing. Cells were treated with *HSF1* shRNA and RA as described above for 24 h before scratch was created with a sterile tip to introduce gaps. Cells were incubated with fresh medium without or with arsenite up to 48 h when wound healing was estimated. Representative phase-contrast images with corresponding treatments as indicated. *Rectangles* represent initial wound boundary. Levels of wound healing with corresponding treatments as indicated on the right. *Error bar*, mean ± S.D. ($n = 3$); ***, $p < 0.001$; *ns*, nonsignificant. *G*, qRT-PCR analysis of the cellular levels of *HSF1*, *HO-1*, and *HSP70* (positive control) mRNA induced by H_2O_2 (100 μM, 3 h). *Error bar*, mean ± S.D. ($n = 3$). *H*, viability of cells determined by MTT assay under treatment conditions as indicated. *Error bar*, mean ± S.D. ($n = 3$); **, $p < 0.01$. *KD*, knockdown/inhibition.

The ARE-C element matched the downstream AGC present in both *NQO1* and *HO-1* AREs but it carries TTA instead of TGA upstream. Assembly of the complex with nuclear extracts on the ARE-B and ARE-C, with mobility similar to that of *NQO1*, suggests the formation of a complex involving similar players (Fig. 4*C*). The K_D value of ARE-C, however, was measured to be two and three times of that of ARE-B and *NQO1*, respectively (Fig. 4*E*). The K_D of NRF2-MafG heterodimer binding to ARE-B with a higher affinity than that of ARE-C suggests that the requirement of GC at 9, 10 position of an ARE may not be essential in all ARE sequence context (36). Although it remains to be experimentally verified, the presence of T at position 3 of ARE-C (which is less conserved in the consensus ARE) may be responsible for its lower affinity to bind the NRF2-MafG heterodimer (Fig. 4*E*). Mismatch in positions 4 and 10 may have rendered putative ARE-A inactive (although r-VISTA scored it higher than ARE-C. (Fig. 2, *B, left panel*, and *C*).

The sensitivity of both NRF2- and HSF1-guided pathways to a proteotoxic stressor is known; HSF1 and NRF2 were shown to activate a common set of genes with overlapping functions in heat shock and antioxidant response pathways (56). NRF2 and HSF1 were reported to compensate for each other's activity (20). NRF2 increase *HSP70* expression during methionine deprivation in a process independent of HSF1 function, suggesting thatinhibitionofHSF1activitycanbeinpartbypassedbyNRF2-dependent antioxidant response (57). *NRF2* knockout mice showed a higher level of unfolded protein response, thus a higher level of HSF1 activation (58). This compensatory function may be responsible for failure to detect any significant change of HSP70 transcription induction in cells with down-regulated *NRF2* (Fig. 3*A*). *HSP70* was also regulated by factors other than HSF1 (29). Although this study convincingly showed that cellular *HSF1* is a target of NRF2, especially under oxidative stress, it remains to be determined why earlier ChIP sequencing studies did not detect NRF2 presence on the *HSF1* promoter (35, 36, 38). Studies here suggest that *HSF1* transcription was differentially regulated by oxidative stress in different cells. For example, it was induced 8-fold more in HT1080 compared with the NKE cells (Fig. 1*B*). Additional investigation is necessary to conclude that the extent of dependence on NRF2 is determined in a cell by its endogenous ROS level. This study shows that *HSF1* gene is up-regulated in cells by oxidative stress in proportion to their endogenous ROS levels (Fig. 1*B*). Efficient neutralization of the effect of arsenite by *N*-acetyl cysteine suggested that a major mediator of arsenite action was through increasing the level of cellular ROS (Fig. 5*C*).

We also found that NRF2 requires BRG1 to regulate *HSF1* promoter activity (Fig. 6). Down-regulation of FACT and helicase-like transcription factor (HLTF) did not affect arsenite-induced *HSF1* transcription. An association of P-TEFb, Mediator, and DNA-bending protein is anticipated in the process. MED16 was shown to be required in NRF2 target gene expression (59). Future studies will show how NRF2, recruited at the identified ARE-B and -C, communicates with RNA polymerase II at the core promoter (60).

This study highlighted an important role of NRF2 and HSF1 collaboration in cancer cells survival and progression. Our results suggested that both NRF2 and HSF1 alone or in combination play a positive role in arsenite-induced EMT and migration in MCF7 cells (Fig. 7, *D–H*) (61). These two factors may support these processes by enhancing autophagy (Fig. 7, *D* and *E*), an important process many cancer cells utilize for their benefit (20, 51, 53, 62).

Many cancer cells have an elevated level of oxidative stress (63). An activated ROS signaling supports prosurvival pathways through facilitating several cellular processes such as inactivating tumor suppressor genes, enhancing glucose consumption, the rate of oncogenic mutation, and anaerobic respiration (64). NRF2 plays a crucial role in maintaining higher ROS in cells. Oncogenes can direct increased *NRF2* expression (65). This gain of function in NRF2-controlled interactome has been reported in lung, breast, skin, esophageal, gallbladder, renal, pancreatic, and endometrial cancer (66, 67). NRF2 exerts checks and balances on the cellular ROS level by up-regulating expression of its target genes such as GSH peroxidase and peroxiredoxin (20, 64). At the same time, cancer cells exhibit an elevated level of HSF1 activity, *i.e.* up-regulated levels of HSPs to support their prosurvival property (15, 16). The role of various posttranslational modifications modulating HSF1 activity has been under extensive investigation (5). Altogether, the results presented here shed light on the molecular basis of transcriptional up-regulation of the *HSF1* gene for adaptation to oxidative stress and its correlation with aggressiveness of cancer.

Experimental procedures

Cell culture

The mammalian cell lines used in this study, HT1080 (human fibrosarcoma), HeLa (cervical carcinoma), MCF7 (breast adenocarcinoma), PC3 (prostate adenocarcinoma), HEK293 (immortalized human embryonic kidney), and NKE (normal kidney epithelium), were a kind gift from Dr. Andrei Gudkov. All cells were grown in complete DMEM (Gibco) supplemented with 10% FBS (Gibco), 2 mM L-glutamine (Himedia), 100 units/ml penicillin-streptomycin (Himedia), 2.5 μg/ml amphotericin B (Himedia), and nonessential amino acids (Himedia). Cells were cultured in 37 °C in a humidified atmosphere containing 5% CO_2. Cells grown to no more than 90% confluence were distributed in new plates by trypsinization as required.

Reagents and antibodies

All the reagents were of analytical grade and were purchased from SRL India, Merck, or Sigma-Aldrich. All primers and oligonucleotides used were procured from Sigma-Aldrich. Restriction enzymes were bought from New England Biolabs. The antibodies used were anti-HSF1 (BioBharati LifeSciences, AB 0220), anti-HSP70 (BioBharati LifeSciences, AB 0210), anti-NRF2 (Cell Signaling Technology, 12721), anti–β-actin HRP secondary (Abcam, ab20272), anti–HO-1 (Cell Signaling Technology, 5853), anti-HLTF (SMARCA3) (Novus, NB100–280), anti-BRG1 (Cell Signaling Technology, 3508), anti-SSRP1 (BioLegend, 609702), anti–E-cadherin (Cell Signaling Technology, 3195), anti–N-cadherin (Cell Signaling Technology, 13116), anti-ATG7 (Cell Signaling Technology, 2631), and anti-LC3B (Cell Signaling Technology, 3868).

Heat shock and arsenite treatments

The cells were plated the day before for treatment. Heat shock was conducted by submerging the plate of cells (grown to ~70% confluency) in water bath pre-warmed at 42 °C for 1 h. The temperature in the medium reached 42 °C within 5 min. The growth medium was not replaced either before or after heat shock. Treatment with sodium arsenite (20 μM) was carried out for 2 h unless otherwise indicated.

Preparation of whole cell extracts and Western blot analysis

The cells were harvested from culture plates with a cell scraper on ice in ice cold PBS and rinsed twice with PBS. Whole cell extracts were prepared essentially using the procedure described earlier (29). Cell extracts containing 20–50 μg total protein or as appropriate were electrophoresed in 10%

(acrylamide:bisacrylamide::29:1) denaturing PAGE and the resolved proteins were transferred to PVDF membrane (EMD Millipore). The membrane was blocked with 3% BSA or 5% fat-free milk in PBST (137 mM NaCl, 2.7 mM KCl, 10 mM Na_2HPO4, 1.8 mM KH_2PO4, pH 7.4, supplemented with 0.1% Tween 20) for 30 min at room temperature and incubated with a desired primary antibody at an optimized dilution for overnight at 4 °C. The next day, the membrane was washed three to four times with PBST followed by incubation with secondary antibody for 1 h at room temperature. The membrane was then washed as before and developed by chemiluminescent detection (Clarity Bio-Rad) according to manufacturer's instructions. For quantification of the immunoblots, band intensities were measured using ImageJ software considering β-actin as normalization control and values were plotted using GraphPad Prism 6.0.

RNA isolation, semiquantitative RT-PCR, and qRT-PCR

Total RNA was isolated from cultured cells using TRIzol reagent as per manufacturer's protocol (Life Technologies). Isolated RNA was dissolved in ultrapure water and quantified using BioSpectrometer (Eppendorf). For cDNA preparation, 1 μg total RNA was reverse transcribed using iScript cDNA Synthesis Kit (Bio-Rad) in 10 μl reaction volume. For semiquantitative RT-PCR, a 10-fold (or as appropriate) diluted cDNA was probed with gene-specific primers using Taq polymerase. Expression of GAPDH mRNA in the same sample under analysis was considered as endogenous control. qRT-PCR was performed using SYBR Green (SYBR Green Hot JumpStart) according to the manufacturer's protocol (Sigma-Aldrich). Results were expressed as the ratio of treated samples to untreated samples normalized to their GAPDH levels. Measured numbers of threshold were converted to relative -fold change using $2^{-\Delta\Delta CT}$ method (68). The primer sets used for estimation of transcript levels for different genes are described in the supporting information (Table S1).

Plasmid constructs

The human *HSP70* promoter (pHSP70 (−450/+91)) and 5′-deletion fragments of the human *HSF1* promoter (Fig. 2) were generated by PCR from human genomic DNA using primers containing restriction sites. An XhoI and HindIII recognition site was added to the PCR product through 5′-ends of forward and reverse primers, respectively. Amplified fragments were subsequently cloned into the pGL4.79 [hRluc/neo] reporter vector (Promega) pre-digested with the same restriction enzymes. Cloning of the ARE site from NQO1 gene promoter (5′-TCCGCAGTCACAGTGACTCAGCAGAATCTG-3′) and *HSF1* promoter versions was done in pGL4.79-mCMV between Acc65I and BglII sites. The pGL4.79-mCMV vector is a modified pGL4.79[hRluc/neo] vector with a minimal CMV (mCMV) enhancer element (5′-TAGAGGGTATATAATG-GAAGCTCGACTTCCAG-3′) cloned between BglII and HindIII sites. Nucleotide sequences of PCR primers used are listed in supporting information (Table S2).

Luciferase reporter assay

HT1080 cells grown in 12-well plates to ~70% confluence were transfected with different reporter constructs carrying the *HSF1* promoter variants using Lipofectamine 2000 (29). Next day, cells were distributed into two wells and treated with or without 20 μM arsenite for 2 h, followed by isolating the RNAs by TRIzol reagent. Expression levels of different genes were measured by semiquantitative RT-PCR and qRT-PCR from the cDNA prepared from the total RNA pretreated with DNase I. Relative -fold increase in Renilla-luciferase (Rluc) mRNA levels in the presence of arsenite was calculated with respect to the untreated control as well as carrier internal vector control. The levels of Rluc mRNA in samples transfected with promoterless pGL4.79 [hRluc/neo] vector was considered as 1. Unless otherwise stated, reporter gene assays were carried out in three parallel experiments or repeated at least three times.

Construction of shNRF2-pLKO.1-puro vector

shRNA (5′-TGGCATCACCAGAACACTCAGTGGAATCT-3′) against the *NRF2* gene was cloned at AgeI/EcoR1 sites in pLKO.1-puro (a third-generation lentiviral vector constructed at Bob Weinberg Lab, Addgene plasmid no. 8453) with the help of RNAi Consortium (TRC) portal (http://www.broadinstitute.org/rnai/public/)[4] (47). For stable knockdown of *NRF2*, cells were transduced by lentiviral particles made from shNRF2-pLKO.1 vector using psPAX2 (Addgene, no. 12260) and pMD2.G (Addgene, no. 12259) as packaging plasmids following the protocol described in the supporting information (69).

EMSA

Nuclear extracts (NE) were prepared from HT1080 cells with NE buffer (25 mM HEPES, pH 7.8, 420 mM NaCl, 10% glycerol, 0.5 mM EDTA, and 1% Nonidet P-40) supplemented with protease and phosphatase inhibitors. ARE-A (5′-CTGGGGG-CTGG AAGAGAAATGGGTCC-3′), ARE-B (5′-GGATTGG-CTGAAGAGTCACAGGAATG-3′), ARE-C (5′-TAGAC-TCTTAGGAAGCAGTTGAAGGC-3′) regions of the *HSF1* promoter or their mutated forms (ARE-mB (5′-GGATTGGC-cacAGAGTCACAGGAATG-3′), ARE-mC (5′-TAGACTCT-cacG AAGCAGTTGAAGGC-3′), and human NQO1-ARE regions (5′-TCCGCAGTCACAGTGACTCA GCAGAAT-CTG-3′)), after annealing with their complementary strands, were end-labeled with [γ-^{32}P]ATP using T4 polynucleotide kinase. Six ng of a probe was incubated with 20 μg of NE on ice for 30 min in a 20 μl reaction in binding buffer (20 mM HEPES, pH 7.9, 100 mM NaCl, 10% glycerol, 0.5 mM EDTA, 2 μg BSA, 2.5 μg salmon sperm DNA, 1 mM PMSF, 1 mM NaF, and 1 mM Na_3VO_4). For competitive binding, a 100-fold excess of respective unlabeled double-stranded WT or mutant oligonucleotides was added to the reaction mixture. For super-shift analysis, anti-NRF2 antibody (1 μg), anti-His_6 antibody (1 μg), or an IgG antibody (1 μg) was added to the reaction mixture. The reaction products were analyzed on a 4% nondenaturating polyacrylamide (acrylamide:bisacrylamide::29:1) gel in TBE buffer (45 mM Tris borate with 1 mM EDTA, pH 8.0). The dried gel was visualized using a Typhoon Trio$^+$ PhosphorImager (GE

Healthcare). DNase I footprinting was performed as described (70).

ChIP assay

HT1080 cells transfected with a FLAG-tagged NRF2 overexpression plasmid (NC16 pCDNA3.1 FLAG, Addgene plasmid no. 36971) were treated with 20 μM sodium arsenite or mock for 2 h. Treatment with *N*-acetyl cysteine (5 mM) was carried out for 3 h prior to treatment with arsenite. Preparation of sheared chromatin, incubation with anti-FLAG antibody (Sigma-Aldrich, F7425) for collecting the associated DNA, and PCR were carried out (31). The DNA was quantified by quantitative PCR using the primers listed in supporting information (Table S3). ChIP against RNA Polymerase II was performed with anti-RNA Polymerase II antibody (Abcam, ab817).

Cell proliferation analysis

Cell proliferation was measured by viability determination using 3-(4,5-dimethylthiazol-2-yl)-2,5-diphenyltetrazolium bromide (MTT) assay or by direct cell counting. Cells were seeded at 0.5×10^5 cells per well in 12-well plates and incubated under standard conditions. After the experiment, cells were incubated with 0.5 mg/ml MTT solution (Himedia, RM1131) at 37 °C, 5% CO_2 for 4 h in the dark. After 4 h incubation the MTT solution was removed and DMSO was added to the plates. A_{570} value was measured with BioSpectrometer (Eppendorf). For counting, cells were trypsinized after washing with PBS. After making thorough suspension, samples were counted using hemocytometer.

Wound healing assay

Cells (2×10^5) were grown in complete medium in 6-well plates until cells were 80–90% confluent. The undersurface of each well was marked with three parallel straight lines. A scratch was made across the surface of the plate using sterilized disposable 200 μl pipette tip to remove the complete layer of cells within the scratch area at 90° to the orientation lines. Each well was then washed twice with PBS, replaced with growth medium supplemented with 5% serum, and treated as mentioned. The width of the scratch was imaged using a microscope with camera (Leica) immediately (0 h) or after 24 or 48 h of treatment at the same magnification settings. Scratch-gap area was measured using ImageJ software and values were plotted using GraphPad Prism 6.0.

ROS quantification by DCFDA assay

Cells pre-treated as appropriate were incubated with 5 μM DCFDA for 30 min. After removing the DCFDA by washing twice with ice-cold PBS, the labeled cells were trypsinized, rinsed, and finally resuspended in PBS. Oxidation of DCFDA to the highly fluorescent 2′,7′-dichlorofluorescein proportional to ROS generation was analyzed by measuring 10,000 events/sample using FACS (BD FACSVerse, BD Biosciences).

Bioinformatics analysis

Transcription factor–binding site analysis was done by rVista (rVista 2.0; https://rvista.dcode.org).[4] WebLogo program (http://weblogo.berkeley.edu)[4] was used for generating the sequence logo of the ARE motif from a curated list of known AREs as described (39).

Statistical analysis

All experiments were performed at least three times. Plotting of graphs and statistical analysis was performed by one-way analysis of variance (ANOVA) with appropriate post hoc tests, using GraphPad Prism 6.0 software. Scatter plots represent individual data points combined with mean ± S.D. Values were considered to be statistically significant when $p < 0.05$.

Author contributions—S. P., S. G., and S. M. data curation; S. P. and S. S. formal analysis; S. P., S. G., S. M., S. S., and M. P. validation; S. P., S. M., and M. P. investigation; S. P. and M. P. visualization; S. P., S. G., and S. S. methodology; S. P. and M. P. writing-original draft; S. S. resources; M. P. conceptualization; M. P. supervision; M. P. project administration; M. P. writing-review and editing.

Acknowledgments—We thank Hozumi Motohashi for sharing the His_6-MafG expression construct and Srabani Pal and Suchandan Bhattacharjee of BioBharati LifeScience for help with NRF2 protein expression. The help of Cheng-Ming Chiang and Donal S. Luse for editing the manuscript is highly appreciated. Our thanks to Abir K. Panda for guidance during rVISTA analysis and Vinod K. Nelson for sharing azadiradione. We thank Asif Ali and Koustav Pal for comments.

References

1. Lindquist, S. (1986) The heat-shock response. *Annu. Rev. Biochem.* **55,** 1151–1191 CrossRef Medline
2. Labbadia, J., and Morimoto, R. I. (2015) The biology of proteostasis in aging and disease. *Annu. Rev. Biochem.* **84,** 435–464 CrossRef Medline
3. Dokladny, K., Myers, O. B., and Moseley, P. L. (2015) Heat shock response and autophagy—cooperation and control. *Autophagy* **11,** 200–213 CrossRef Medline
4. Hahn, J. S., Hu, Z., Thiele, D. J., and Iyer, V. R. (2004) Genome-wide analysis of the biology of stress responses through heat shock transcription factor. *Mol. Cell. Biol.* **24,** 5249–5256 CrossRef Medline
5. Li, J., Labbadia, J., and Morimoto, R. I. (2017) Rethinking HSF1 in stress, development, and organismal health. *Trends Cell Biol.* **27,** 895–905 CrossRef Medline
6. Trinklein, N. D., Murray, J. I., Hartman, S. J., Botstein, D., and Myers, R. M. (2004) The role of heat shock transcription factor 1 in the genome-wide regulation of the mammalian heat shock response. *Mol. Biol. Cell* **15,** 1254–1261 CrossRef Medline
7. Morimoto, R. I. (1998) Regulation of the heat shock transcriptional response: Cross talk between a family of heat shock factors, molecular chaperones, and negative regulators. *Genes Dev.* **12,** 3788–3796 CrossRef Medline
8. Shi, Y., Mosser, D. D., and Morimoto, R. I. (1998) Molecular chaperones as HSF1-specific transcriptional repressors. *Genes Dev.* **12,** 654–666 CrossRef Medline
9. Vihervaara, A., and Sistonen, L. (2014) HSF1 at a glance. *J. Cell Sci.* **127,** 261–266 CrossRef Medline
10. Guo, Y., Guettouche, T., Fenna, M., Boellmann, F., Pratt, W. B., Toft, D. O., Smith, D. F., and Voellmy, R. (2001) Evidence for a mechanism of repression of heat shock factor 1 transcriptional activity by a multichaperone complex. *J. Biol. Chem.* **276,** 45791–45799 CrossRef Medline
11. Shamovsky, I., and Nudler, E. (2008) New insights into the mechanism of heat shock response activation. *Cell. Mol. Life Sci.* **65,** 855–861 CrossRef Medline
12. Thomson, S., Hollis, A., Hazzalin, C. A., and Mahadevan, L. C. (2004) Distinct stimulus-specific histone modifications at hsp70 chromatin tar-

geted by the transcription factor heat shock factor-1. *Mol. Cell* **15,** 585–594 CrossRef Medline
13. Dai, C., Dai, S., and Cao, J. (2012) Proteotoxic stress of cancer: Implication of the heat-shock response in oncogenesis. *J. Cell. Physiol.* **227,** 2982–2987 CrossRef Medline
14. Manda, G., Isvoranu, G., Comanescu, M. V., Manea, A., Debelec Butuner, B., and Korkmaz, K. S. (2015) The redox biology network in cancer pathophysiology and therapeutics. *Redox Biol.* **5,** 347–357 CrossRef Medline
15. Dai, C., Whitesell, L., Rogers, A. B., and Lindquist, S. (2007) Heat shock factor 1 is a powerful multifaceted modifier of carcinogenesis. *Cell* **130,** 1005–1018 CrossRef Medline
16. Calderwood, S. K. (2012) HSF1, a versatile factor in tumorogenesis. *Curr. Mol. Med.* **12,** 1102–1107 CrossRef Medline
17. Ishiwata, J., Kasamatsu, A., Sakuma, K., Iyoda, M., Yamatoji, M., Usukura, K., Ishige, S., Shimizu, T., Yamano, Y., Ogawara, K., Shiiba, M., Tanzawa, H., and Uzawa, K. (2012) State of heat shock factor 1 expression as a putative diagnostic marker for oral squamous cell carcinoma. *Int. J. Oncol.* **40,** 47–52 CrossRef Medline
18. Fang, F., Chang, R., and Yang, L. (2012) Heat shock factor 1 promotes invasion and metastasis of hepatocellular carcinoma in vitro and in vivo. *Cancer* **118,** 1782–1794 CrossRef Medline
19. Santagata, S., Hu, R., Lin, N. U., Mendillo, M. L., Collins, L. C., Hankinson, S. E., Schnitt, S. J., Whitesell, L., Tamimi, R. M., Lindquist, S., and Ince, T. A. (2011) High levels of nuclear heat-shock factor 1 (HSF1) are associated with poor prognosis in breast cancer. *Proc. Natl. Acad. Sci. U.S.A.* **108,** 18378–18383 CrossRef Medline
20. Dayalan Naidu, S., Kostov, R. V., and Dinkova-Kostova, A. T. (2015) Transcription factors Hsf1 and Nrf2 engage in crosstalk for cytoprotection. *Trends Pharmacol. Sci.* **36,** 6–14 CrossRef Medline
21. Kensler, T. W., Wakabayashi, N., and Biswal, S. (2007) Cell survival responses to environmental stresses via the Keap1-Nrf2-ARE pathway. *Annu. Rev. Pharmacol. Toxicol.* **47,** 89–116 CrossRef Medline
22. Suzuki, T., and Yamamoto, M. (2015) Molecular basis of the Keap1-Nrf2 system. *Free Radic. Biol. Med.* **88,** 93–100 CrossRef Medline
23. Hayes, J. D., and Dinkova-Kostova, A. T. (2014) The Nrf2 regulatory network provides an interface between redox and intermediary metabolism. *Trends Biochem. Sci.* **39,** 199–218 CrossRef Medline
24. McMahon, M., Lamont, D. J., Beattie, K. A., and Hayes, J. D. (2010) Keap1 perceives stress via three sensors for the endogenous signaling molecules nitric oxide, zinc, and alkenals. *Proc. Natl. Acad. Sci. U.S.A.* **107,** 18838–18843 CrossRef Medline
25. Taguchi, K., and Yamamoto, M. (2017) The KEAP1-NRF2 system in cancer. *Front. Oncol.* **7,** 85 CrossRef Medline
26. Maines, M. D., and Ewing, J. F. (1996) Stress response of the rat testis: In situ hybridization and immunohistochemical analysis of heme oxygenase-1 (HSP32) induction by hyperthermia. *Biol. Reprod.* **54,** 1070–1079 CrossRef Medline
27. Prestera, T., Talalay, P., Alam, J., Ahn, Y. I., Lee, P. J., and Choi, A. M. (1995) Parallel induction of heme oxygenase-1 and chemoprotective phase 2 enzymes by electrophiles and antioxidants: Regulation by upstream antioxidant-responsive elements (ARE). *Mol. Med.* **1,** 827–837 CrossRef Medline
28. Almeida, D. V., da Silva Nornberg, B. F., Geracitano, L. A., Barros, D. M., Monserrat, J. M., and Marins, L. F. (2010) Induction of phase II enzymes and *hsp70* genes by copper sulfate through the electrophile-responsive element (*EpRE*): Insights obtained from a transgenic zebrafish model carrying an orthologous *EpRE* sequence of mammalian origin. *Fish Physiol. Biochem.* **36,** 347–353 CrossRef Medline
29. Hazra, J., Mukherjee, P., Ali, A., Poddar, S., and Pal, M. (2017) Engagement of components of DNA-break repair complex and NFκB in Hsp70A1A transcription upregulation by heat shock. *PLoS One* **12,** e0168165 CrossRef Medline
30. Sasi, B. K., Sonawane, P. J., Gupta, V., Sahu, B. S., and Mahapatra, N. R. (2014) Coordinated transcriptional regulation of Hspa1a gene by multiple transcription factors: Crucial roles for HSF-1, NF-Y, NF-κB, and CREB. *J. Mol. Biol.* **426,** 116–135 CrossRef Medline
31. Jain, A., Lamark, T., Sjøttem, E., Larsen, K. B., Awuh, J. A., Øvervatn, A., McMahon, M., Hayes, J. D., and Johansen, T. (2010) p62/SQSTM1 is a target gene for transcription factor NRF2 and creates a positive feedback loop by inducing antioxidant response element-driven gene transcription. *J. Biol. Chem.* **285,** 22576–22591 CrossRef Medline
32. Padmanabhan, B., Tong, K. I., Ohta, T., Nakamura, Y., Scharlock, M., Ohtsuji, M., Kang, M. I., Kobayashi, A., Yokoyama, S., and Yamamoto, M. (2006) Structural basis for defects of Keap1 activity provoked by its point mutations in lung cancer. *Mol. Cell* **21,** 689–700 CrossRef Medline
33. Wakabayashi, N., Shin, S., Slocum, S. L., Agoston, E. S., Wakabayashi, J., Kwak, M. K., Misra, V., Biswal, S., Yamamoto, M., and Kensler, T. W. (2010) Regulation of notch1 signaling by nrf2: Implications for tissue regeneration. *Sci. Signal.* **3,** ra52 CrossRef Medline
34. Lau, A., Whitman, S. A., Jaramillo, M. C., and Zhang, D. D. (2013) Arsenic-mediated activation of the Nrf2-Keap1 antioxidant pathway. *J. Biochem. Mol. Toxicol.* **27,** 99–105 CrossRef Medline
35. Chorley, B. N., Campbell, M. R., Wang, X., Karaca, M., Sambandan, D., Bangura, F., Xue, P., Pi, J., Kleeberger, S. R., and Bell, D. A. (2012) Identification of novel NRF2-regulated genes by ChIP-Seq: Influence on retinoid X receptor alpha. *Nucleic Acids Res.* **40,** 7416–7429 CrossRef Medline
36. Hirotsu, Y., Katsuoka, F., Funayama, R., Nagashima, T., Nishida, Y., Nakayama, K., Engel, J. D., and Yamamoto, M. (2012) Nrf2-MafG heterodimers contribute globally to antioxidant and metabolic networks. *Nucleic Acids Res.* **40,** 10228–10239 CrossRef Medline
37. Kimura, M., Yamamoto, T., Zhang, J., Itoh, K., Kyo, M., Kamiya, T., Aburatani, H., Katsuoka, F., Kurokawa, H., Tanaka, T., Motohashi, H., and Yamamoto, M. (2007) Molecular basis distinguishing the DNA binding profile of Nrf2-Maf heterodimer from that of Maf homodimer. *J. Biol. Chem.* **282,** 33681–33690 CrossRef Medline
38. Malhotra, D., Portales-Casamar, E., Singh, A., Srivastava, S., Arenillas, D., Happel, C., Shyr, C., Wakabayashi, N., Kensler, T. W., Wasserman, W. W., and Biswal, S. (2010) Global mapping of binding sites for Nrf2 identifies novel targets in cell survival response through ChIP-Seq profiling and network analysis. *Nucleic Acids Res.* **38,** 5718–5734 CrossRef Medline
39. Wang, X., Tomso, D. J., Chorley, B. N., Cho, H. Y., Cheung, V. G., Kleeberger, S. R., and Bell, D. A. (2007) Identification of polymorphic antioxidant response elements in the human genome. *Hum. Mol. Genet.* **16,** 1188–1200 CrossRef Medline
40. Imhoff, B. R., and Hansen, J. M. (2010) Tert-butylhydroquinone induces mitochondrial oxidative stress causing Nrf2 activation. *Cell Biol. Toxicol.* **26,** 541–551 CrossRef Medline
41. Nelson, V. K., Ali, A., Dutta, N., Ghosh, S., Jana, M., Ganguli, A., Komarov, A., Paul, S., Dwivedi, V., Chatterjee, S., Jana, N. R., Lakhotia, S. C., Chakrabarti, G., Misra, A. K., Mandal, S. C., and Pal, M. (2016) Azadiradione ameliorates polyglutamine expansion disease in Drosophila by potentiating DNA binding activity of heat shock factor 1. *Oncotarget* **7,** 78281–78296 CrossRef Medline
42. Katoh, Y., Itoh, K., Yoshida, E., Miyagishi, M., Fukamizu, A., and Yamamoto, M. (2001) Two domains of Nrf2 cooperatively bind CBP, a CREB binding protein, and synergistically activate transcription. *Genes Cells* **6,** 857–868 CrossRef Medline
43. Tebay, L. E., Robertson, H., Durant, S. T., Vitale, S. R., Penning, T. M., Dinkova-Kostova, A. T., and Hayes, J. D. (2015) Mechanisms of activation of the transcription factor Nrf2 by redox stressors, nutrient cues, and energy status and the pathways through which it attenuates degenerative disease. *Free Radic. Biol. Med.* **88,** 108–146 CrossRef Medline
44. Nioi, P., Nguyen, T., Sherratt, P. J., and Pickett, C. B. (2005) The carboxy-terminal Neh3 domain of Nrf2 is required for transcriptional activation. *Mol. Cell. Biol.* **25,** 10895–10906 CrossRef Medline
45. Zhang, J., Ohta, T., Maruyama, A., Hosoya, T., Nishikawa, K., Maher, J. M., Shibahara, S., Itoh, K., and Yamamoto, M. (2006) BRG1 interacts with Nrf2 to selectively mediate HO-1 induction in response to oxidative stress. *Mol. Cell. Biol.* **26,** 7942–7952 CrossRef Medline
46. Gökmen-Polar, Y., and Badve, S. (2016) Upregulation of HSF1 in estrogen receptor positive breast cancer. *Oncotarget* **7,** 84239–84245 CrossRef Medline
47. Wang, X. J., Sun, Z., Chen, W., Eblin, K. E., Gandolfi, J. A., and Zhang, D. D. (2007) Nrf2 protects human bladder urothelial cells from arsenite

and monomethylarsonous acid toxicity. *Toxicol. Appl. Pharmacol.* **225,** 206–213 CrossRef Medline

48. Mani, S. A., Guo, W., Liao, M. J., Eaton, E. N., Ayyanan, A., Zhou, A. Y., Brooks, M., Reinhard, F., Zhang, C. C., Shipitsin, M., Campbell, L. L., Polyak, K., Brisken, C., Yang, J., and Weinberg, R. A. (2008) The epithelial-mesenchymal transition generates cells with properties of stem cells. *Cell* **133,** 704–715 CrossRef Medline
49. Creighton, C. J., Chang, J. C., and Rosen, J. M. (2010) Epithelial-mesenchymal transition (EMT) in tumor-initiating cells and its clinical implications in breast cancer. *J. Mammary Gland Biol. Neoplasia* **15,** 253–260 CrossRef Medline
50. Gravdal, K., Halvorsen, O. J., Haukaas, S. A., and Akslen, L. A. (2007) A switch from E-cadherin to N-cadherin expression indicates epithelial to mesenchymal transition and is of strong and independent importance for the progress of prostate cancer. *Clin. Cancer Res.* **13,** 7003–7011 CrossRef Medline
51. Gugnoni, M., Sancisi, V., Manzotti, G., Gandolfi, G., and Ciarrocchi, A. (2016) Autophagy and epithelial-mesenchymal transition: An intricate interplay in cancer. *Cell Death Dis.* **7,** e2520 CrossRef Medline
52. Tanida, I., Ueno, T., and Kominami, E. (2008) LC3 and autophagy. *Methods Mol. Biol.* **445,** 77–88 CrossRef Medline
53. Desai, S., Liu, Z., Yao, J., Patel, N., Chen, J., Wu, Y., Ahn, E. E., Fodstad, O., and Tan, M. (2013) Heat shock factor 1 (HSF1) controls chemoresistance and autophagy through transcriptional regulation of autophagy-related protein 7 (ATG7). *J. Biol. Chem.* **288,** 9165–9176 CrossRef Medline
54. Fung, C., Lock, R., Gao, S., Salas, E., and Debnath, J. (2008) Induction of autophagy during extracellular matrix detachment promotes cell survival. *Mol. Biol. Cell* **19,** 797–806 CrossRef Medline
55. Yoo, N. J., Kim, H. R., Kim, Y. R., An, C. H., and Lee, S. H. (2012) Somatic mutations of the KEAP1 gene in common solid cancers. *Histopathology* **60,** 943–952 CrossRef Medline
56. Zhang, L., Pang, E., Loo, R. R., Rao, J., Go, V. L., Loo, J. A., and Lu, Q. Y. (2011) Concomitant inhibition of HSP90, its mitochondrial localized homologue TRAP1 and HSP27 by green tea in pancreatic cancer HPAF-II cells. *Proteomics* **11,** 4638–4647 CrossRef Medline
57. Hensen, S. M., Heldens, L., van Enckevort, C. M., van Genesen, S. T., Pruijn, G. J., and Lubsen, N. H. (2013) Activation of the antioxidant response in methionine deprived human cells results in an HSF1-independent increase in HSPA1A mRNA levels. *Biochimie* **95,** 1245–1251 CrossRef Medline
58. Meakin, P. J., Chowdhry, S., Sharma, R. S., Ashford, F. B., Walsh, S. V., McCrimmon, R. J., Dinkova-Kostova, A. T., Dillon, J. F., Hayes, J. D., and Ashford, M. L. (2014) Susceptibility of Nrf2-null mice to steatohepatitis and cirrhosis upon consumption of a high-fat diet is associated with oxidative stress, perturbation of the unfolded protein response, and disturbance in the expression of metabolic enzymes but not with insulin resistance. *Mol. Cell. Biol.* **34,** 3305–3320 CrossRef Medline
59. Sekine, H., Okazaki, K., Ota, N., Shima, H., Katoh, Y., Suzuki, N., Igarashi, K., Ito, M., Motohashi, H., and Yamamoto, M. (2016) The mediator subunit MED16 transduces NRF2-activating signals into antioxidant gene expression. *Mol. Cell. Biol.* **36,** 407–420 CrossRef Medline
60. Thanos, D., and Maniatis, T. (1995) Virus induction of human IFNβ gene expression requires the assembly of an enhanceosome. *Cell* **83,** 1091–1100 CrossRef Medline
61. Arfmann-Knübel, S., Struck, B., Genrich, G., Helm, O., Sipos, B., Sebens, S., and Schäfer, H. (2015) The crosstalk between Nrf2 and TGF-β1 in the epithelial-mesenchymal transition of pancreatic duct epithelial cells. *PLoS One* **10,** e0132978 CrossRef Medline
62. Rojo de la Vega, M., Chapman, E., and Zhang, D. D. (2018) NRF2 and the hallmarks of cancer. *Cancer Cell* **34,** 21–43 CrossRef Medline
63. Panieri, E., and Santoro, M. M. (2016) ROS homeostasis and metabolism: A dangerous liaison in cancer cells. *Cell Death Dis.* **7,** e2253 CrossRef Medline
64. Moloney, J. N., and Cotter, T. G. (2017) ROS signalling in the biology of cancer. *Semin. Cell Dev. Biol.* **80,** 50–64 CrossRef Medline
65. DeNicola, G. M., Karreth, F. A., Humpton, T. J., Gopinathan, A., Wei, C., Frese, K., Mangal, D., Yu, K. H., Yeo, C. J., Calhoun, E. S., Scrimieri, F., Winter, J. M., Hruban, R. H., Iacobuzio-Donahue, C., Kern, S. E., Blair, I. A., and Tuveson, D. A. (2011) Oncogene-induced Nrf2 transcription promotes ROS detoxification and tumorigenesis. *Nature* **475,** 106–109 CrossRef Medline
66. Jiang, T., Chen, N., Zhao, F., Wang, X. J., Kong, B., Zheng, W., and Zhang, D. D. (2010) High levels of Nrf2 determine chemoresistance in type II endometrial cancer. *Cancer Res.* **70,** 5486–5496 CrossRef Medline
67. Shibata, T., Ohta, T., Tong, K. I., Kokubu, A., Odogawa, R., Tsuta, K., Asamura, H., Yamamoto, M., and Hirohashi, S. (2008) Cancer related mutations in NRF2 impair its recognition by Keap1-Cul3 E3 ligase and promote malignancy. *Proc. Natl. Acad. Sci. U.S.A.* **105,** 13568–13573 CrossRef Medline
68. Livak, K. J., and Schmittgen, T. D. (2001) Analysis of relative gene expression data using real-time quantitative PCR and the $2^{-\Delta\Delta CT}$ method. *Methods* **25,** 402–408 CrossRef Medline
69. Naldini, L., Blömer, U., Gallay, P., Ory, D., Mulligan, R., Gage, F. H., Verma, I. M., and Trono, D. (1996) In vivo gene delivery and stable transduction of nondividing cells by a lentiviral vector. *Science* **272,** 263–267 CrossRef Medline
70. Carey, M. F., Peterson, C. L., and Smale, S. T. (2013) DNase I footprinting. *Cold Spring Harb. Protoc.* **2013,** 469–478 CrossRef Medline
71. Loots, G., and Ovcharenko, I. (2004) rVista 2.0: Evolutionary analysis of transcription factor binding sites. *Nucleic Acids Res.* **32,** W217–W221 CrossRef Medline